

Equilibrium organization, conformation, and dynamics of two polymers under box-like confinement

James M. Polson and Desiree A. Rehel¹

Department of Physics, University of Prince Edward Island, 550 University Avenue, Charlottetown, Prince Edward Island, C1A 4P3, Canada

(Dated: 19 May 2021)

Motivated by recent nanofluidics experiments, we use Brownian dynamics and Monte Carlo simulations to study the conformation, organization and dynamics of two polymer chains confined to a single box-like cavity. The polymers are modeled as flexible hard-sphere chains, and the box has a square cross-section of side length L and a height that is small enough to compress the polymers in that dimension. For sufficiently large L , the system behaviour approaches that of an isolated polymer in a slit. However, the combined effects of crowding and confinement on the polymer organization, conformation and equilibrium dynamics become significant when $L/R_{g,xy}^* \lesssim 5$, where $R_{g,xy}^*$ is the transverse radius of gyration for a slit geometry. In this regime, the centre-of-mass probability distribution in the transverse plane exhibits a depletion zone near the centre of the cavity (except at very small L) and a 4-fold symmetry with quasi-discrete positions. Reduction in polymer size with decreasing L arises principally from confinement rather than inter-polymer crowding. By contrast, polymer diffusion and internal motion are strongly affected by inter-polymer crowding. The two polymers tend to occupy opposite positions relative to the box centre, about which they diffuse relatively freely. Qualitatively, this static and dynamical behaviour differs significantly from that previously observed for confinement of two polymers to a narrow channel. The simulation results for a suitably chosen box width are qualitatively consistent with results from a recent experimental study of two λ -DNA chains confined to a nanofluidic cavity.

I. INTRODUCTION

Nanoscale confinement of a polymer strongly affects its conformational and dynamical properties. Recent advances in nanofabrication techniques have facilitated the creation of lab-on-a-chip nanofluidic devices that are ideal for studying and characterizing such physical effects. In recent years, nanofluidics experiments employing optical imaging techniques to study biopolymers such as DNA have been instrumental in testing and refining decades-old theories of confined polymers. A notable example is confinement of DNA in nanochannels.^{1,2} A thorough understanding of the fundamental physics of such systems is vital for various applications that require stretching of DNA in channels, including DNA sorting,³ DNA denaturation mapping,^{4,5} and genome mapping.⁶⁻⁹ A number of other studies have examined the confinement effects on DNA in embedded nanotopography devices composed of a nanoslit with nanogrooves or nanopits etched into one surface deeper than the surrounding slit. While the pits and grooves generally promote entropic trapping of the DNA, some portion of the contour of the molecule can occupy the narrow region of the slit outside these structures. This enables a novel means for conformational manipulation of single polymers. For example, recent experiments by Reisner and coworkers have observed and characterized ‘digitized’ or ‘tetris’-like conformations for polymers that share their contour between multiple adjacent nanopits.^{10,11} Embedded nanotopography devices can also serve as useful models to characterize single-molecule transport across free energy landscapes.¹²⁻¹⁸

One notable study using nanofluidics techniques to

study the effects of nanoconfinement on polymers was reported recently by Capaldi *et al.*¹⁹ Their experiment employed pneumatic pressure to deflect a thin nitride lid into a nanoslit containing a solution of fluorescently stained λ -DNA chains, forcing the molecules into an array of nanocavities embedded in one surface of the slit. Each cavity had a square cross section of side length $2 \mu\text{m}$, was 200 nm deep, and was able to trap up to two λ -DNA chains per cavity. Differential staining of the chains enabled monitoring of individual chain conformation, the degree of partitioning or mixing of the chains, and coupled diffusion of the centre-of-mass chain positions. Comparing the results to those for cavities with a single trapped DNA chain, the drastic impact of the presence of a second chain on the conformation and dynamics was quantified. Similar, though less pronounced, effects were observed for a cavity-confined system containing a single λ -DNA chain together with a small plasmid.

Numerous theoretical and simulation studies have examined the mixing/partitioning behaviour of two polymers confined to nanoscale cavities and channels in recent years.²⁰⁻⁴⁰ Under sufficiently strong confinement, polymers tend to segregate due to entropic repulsion between the chains. It has been suggested that this effect may contribute to the driving force for chromosome segregation in self-replicating bacteria,^{20,41-44} and recent experimental studies have reported results consistent with this hypothesis.^{42,44-48} Unfortunately, *in vivo* experiments on replicating bacteria do not provide a straightforward means to quantify the degree of entropic repulsion. By contrast, *in vitro* nanofluidics experiments such as that by Capaldi *et al.*, which consider much simpler systems, are much better suited for direct comparison with the

predictions of theory and simulation.

In this study, we use Brownian dynamics (BD) and Monte Carlo (MC) simulations to study the organization, conformational behaviour, and equilibrium dynamics of a system of two polymers under confinement in a box-like cavity. Ideally, the molecular model should incorporate correct length scale ratios for the width, contour length, and persistence length of λ -DNA. However, this choice leads to simulations that are far too time consuming to be of practical benefit, especially in the case of dynamics. Consequently, we employ instead a simple coarse-grained molecular model, in which the polymers are described as relatively short flexible chains of spherical Lennard-Jones beads. One goal of this study is to determine whether the general trends observed in the study of Capaldi *et al.* can be accounted for using such a simplistic model. The simulations also provide a means to test the validity of the interpretation proposed by Capaldi *et al.* for the observed dynamical behaviour. In addition, we examine effects of varying system parameters not considered in the experiments. Most notably, we study the effects of varying the confining box dimensions on the polymer dynamics and organization. For sufficiently small cavities, we find that the polymers tend to segregate to opposite sides of the box and that the rates of polymer diffusion and internal motion are both strongly affected by interpolymer crowding. These observations are qualitatively consistent with those of the experimental study, demonstrating the utility of the very simplistic model employed in the simulations. The observed behaviour in this model system may also be of value in interpreting results of future experiments.

The remainder of this article is organized as follows. Section II presents a brief description of the model used in the simulations, following which Section III gives an outline of the methodology employed together with the relevant details of the simulations. Section IV presents the simulation results for the various systems we have examined, and Section V describes the relevance of the simulation results to experiment. Finally, Section VI summarizes the main conclusions of this work.

II. MODEL

We examine systems of either one or two polymer chains confined to a box-like cavity. Each polymer is a flexible linear chain of N spherical monomers. Polymer lengths are in the range $N=40$ – 80 for BD simulations and 40 – 300 for MC simulations. For the two-polymer systems, the lengths of the two polymers are equal. Non-bonded interactions are given by the repulsive Lennard-Jones potential,

$$u_{\text{nb}}(r) = \begin{cases} u_{\text{LJ}}(r) - u_{\text{LJ}}(r_c), & r \leq r_c \\ 0, & r \geq r_c \end{cases} \quad (1)$$

where r is the distance between the monomer centres, $r_c \equiv 2^{1/6}\sigma$, and where $u_{\text{LJ}}(r)$ is the standard Lennard-

Jones 6-12 potential,

$$u_{\text{LJ}}(r) = 4\epsilon \left[\left(\frac{\sigma}{r} \right)^{12} - \left(\frac{\sigma}{r} \right)^6 \right]. \quad (2)$$

Bonded monomers interact with a combination of the potential in Eq. (1) and the finite extensible nonlinear elastic (FENE) potential,

$$u_{\text{FENE}}(r) = -\frac{1}{2}kr_0^2 \ln(1 - (r/r_0)^2), \quad (3)$$

where we choose $k\sigma^2/\epsilon = 30$ and where $r_0 = 1.5\sigma$.

The polymers are enclosed in a rectangular box with a square cross section in the $x - y$ plane of side length L and a height h in the z direction. The box dimensions are defined such that L is the range of positions along the x and y axes accessible to the centres of the monomers, and h is the corresponding range along z . To impose this condition, each monomer interacts with each wall through Eq. (1), where $r + \sigma$ is the distance of the monomer to the nearest point on the wall. Most calculations used $h=4$, a value that is low enough to compress the polymer along the z direction, as was the case in the experiments of Ref. 19. We use a wide range of values for the box width.

III. METHODS

We use two different simulation methods to study the confined-polymer system. BD simulations are used to monitor the dynamics of centre of mass motion as well as the internal dynamics of each chain. Since the focus is on characterizing dynamics at longer time scales, results obtained using the BD method are not expected to differ significantly from those obtained using the more computationally costly Langevin dynamics method. MC simulations employing the standard Metropolis method are used to measure probability distributions associated with polymer position, as well as to characterize the conformational statistics. Although in principle BD simulations could also be used for these measurements, they were far too computationally costly for larger N to obtain statistically sound results in a reasonable time. By contrast, this presented no problem for the much more efficient MC simulations. For convenience, we chose to use MC simulations for the static quantities for all N . Both methods employ the molecular model described in Section II. A brief description of each method follows below.

A. Monte Carlo simulations

We use a standard MC simulation method in which polymer configurations are generated using trial moves that are accepted or rejected based on the Metropolis MC criterion. The trial moves consist of a combination of single-monomer crankshaft rotations, reptation moves

and whole-polymer displacements. The type of each trial move is randomly selected. A single MC cycle consists of $2N$ trial moves, each consisting of $N - 1$ crankshaft moves, $N - 1$ reptation moves, and two whole-polymer translations. For each crankshaft move, a randomly selected monomer was rotated about an axis connecting adjacent monomers through a random angle drawn from uniform distribution in the range $[-\Delta\phi_{\max}, +\Delta\phi_{\max}]$. In the case of end monomers, rotation was about the second bond from the end. Whole-polymer translation was achieved by moving all monomers of a randomly selected polymer through a displacement drawn from a uniform distribution in the range $[-\Delta_{\max}, +\Delta_{\max}]$ for each coordinate. The parameters $\Delta\phi_{\max}$ and Δ_{\max} were chosen to achieve an acceptance ratio of approximately 50%. For each reptation move, the polymer and the reptation direction were both randomly selected.

For each system size, as defined by N and L , we carried out numerous simulations on an array of processors, each using a different sequence of random numbers, to acquire a collection of statistically uncorrelated results. This collection of results was then averaged. Dividing the calculation into such independent runs essentially parallelizes the simulation and dramatically increases the computational efficiency. Each simulation consisted of an equilibration period of typically 10^6 MC cycles followed by a production run of 10^8 MC cycles. The number of these simulations ranged from 50 for $N=40$ to 1000 for $N=300$, corresponding to total simulation times of 540 CPU-hours for $N=40$ to 15000 CPU-hours for $N=300$, respectively.

B. Brownian dynamics simulations

The BD simulations used to study the polymer dynamics employ standard methods. The coordinates of the i th particle are advanced through a time Δt according to the algorithm:

$$x_i(t + \Delta t) = x_i(t) + \frac{f_{i,x}}{\gamma_0} + \sqrt{2k_B T \Delta t / \gamma_0} \Delta w, \quad (4)$$

and likewise for y_i and z_i . Here, $f_{i,x}$ is the x -component of the conservative force on particle i , and γ_0 is the friction coefficient of each monomer. The conservative force is calculated as $f_{i,\alpha} = -\nabla_{i,\alpha} U_{\text{tot}}$, where $\nabla_{i,\alpha}$ is the α -component of the gradient with respect to the coordinates of the i th particle of the total potential energy of the system, U_{tot} . In addition, Δw is a random quantity drawn from a Gaussian of unit variance.

All simulations were carried out at a temperature $T = \epsilon/k_B$, where k_B is Boltzmann's constant. The time step used in Eq. (4) was $\Delta t = 0.0001\tau_{\text{BD}}$, where $\tau_{\text{BD}} \equiv \gamma_0 \sigma^2 / \epsilon$. The run time of each simulation was typically $10^5 \tau_{\text{BD}}$, following an equilibration period of typically $10^4 \tau_{\text{BD}}$. For each system size, as defined by N and L , the results of numerous simulations were averaged and used to estimate uncertainties. This ranged

from 750 simulations for $N=40$ to 1000 simulations for $N=80$, corresponding to total simulation times of roughly 10000 CPU-hours and 30000 CPU-hours, respectively.

C. Measured quantities

To track the polymer centre-of-mass motion, we use the mean-square displacement,

$$\text{MSD}(t) = \left\langle (x_i(t) - x_i(0))^2 \right\rangle. \quad (5)$$

where x_i is the centre-of-mass x coordinate for the i th polymer. The angular brackets denote an average over sequences of configurations generated in separate simulations, as well as over the time origin for each simulation. In addition, an average was carried out over both polymer positions in the 2-polymer system, as well as over the y coordinates of the centres of mass. The latter average is valid since the box width in the x and y dimensions is equal.

A related measure of polymer motion is the position autocorrelation function,

$$C_{\text{auto}}(t) \equiv \langle x_i(t)x_i(0) \rangle. \quad (6)$$

Note that since the box centre lies at $x = 0$, then $\langle x_i \rangle = 0$, and thus $\langle x_i(t)x_i(0) \rangle = \langle x_i^2 \rangle - \frac{1}{2}\text{MSD}(t)$. Correlations between the centre-of-mass kinetics of the two polymers is quantified by the cross-correlation function,

$$C_{\text{cross}}(t) \equiv -\langle x_1(t)x_2(0) \rangle, \quad (7)$$

where the subscripts denote different polymers. Since the signs of x_1 and x_2 tend to be opposite (i.e. the polymers tend to be situated on opposite sides of the box), the negative sign leads to the property, $C_{\text{cross}}(t) \geq 0$.

To examine internal motion of the polymers, we use Rouse coordinates, defined as

$$\mathbf{R}_p \equiv \frac{1}{N} \sum_{n=1}^N \mathbf{r}_n \cos\left(\frac{p(n - \frac{1}{2})\pi}{N}\right), \quad (8)$$

where \mathbf{r}_n is the position of particle n , and $p = 1, 2, 3, \dots$. These are used to calculate the correlation functions

$$C_p(t) = \langle \mathbf{R}_p(t + t_0) \cdot \mathbf{R}_p(t_0) \rangle_{xy}, \quad (9)$$

where the subscript indicates that only transverse components of the coordinates are used in the calculation of the average. In most cases we find that the correlation function decays exponentially such that $C_p \propto e^{-t/\tau_p}$, where τ_p is the correlation time for the p th mode. Typically, we observe a small transient at short times, which is excluded from the fit. The consistently exponential form of $C_p(t)$ for both one- and two-polymer systems with excluded volume under even strong confinement conditions is a somewhat surprising but useful property. For example, we find that the $p = 1$ mode provides a more convenient probe of large-scale conformational changes

than, e.g., the end-to-end displacement since the correlation function of the latter tends not to be exponential under the conditions examined here.

As a measurement of the polymer shape isometry, we use the 2-D version of asphericity, A_2 , defined as

$$A_2 = \frac{\langle R_1^2 \rangle - \langle R_2^2 \rangle}{\langle R_1^2 \rangle + \langle R_2^2 \rangle}, \quad (10)$$

where the angular brackets denote an average over sampled configurations. The quantities R_1^2 and R_2^2 ($\leq R_1^2$) are eigenvalues of the 2-D gyration matrix, whose elements are defined

$$S_{\alpha\beta} = \frac{1}{N} \sum_{i=1}^N (r_{\alpha,i} - r_{\alpha,\text{cm}})(r_{\beta,i} - r_{\beta,\text{cm}}), \quad (11)$$

where $r_{\alpha,i}$ is the α -coordinate ($\alpha = x, y$) of particle i and $r_{\alpha,\text{cm}}$ is the instantaneous α -coordinate of the centre-of-mass. The quantities R_1 and R_2 ($\leq R_1$) can be viewed as the semi-major and semi-minor axes of an equivalent ellipse that very roughly approximates the shape of the polymer in the $x - y$ plane. Note the two limiting cases for the asphericity: $A_2 = 0$ corresponds to a circular disk, and $A_2 = 1$ corresponds to an infinitesimally thin needle. Note as well that $R_{g,xy}^2 = R_1^2 + R_2^2$ is the instantaneous square radius of gyration in the $x - y$ plane. As a measure of inter-polymer overlap, we define the overlap parameter $\chi_{\text{ov}} \equiv N_{\text{ov}}/N$, where N_{ov} is the average number of monomers per polymer that lie inside the overlap area of the two equivalent ellipses defined above.

In the results presented below, distances are measured in units of σ , energy is measured in units of ϵ ($= k_B T$), and time is measured in units of $\gamma_0 \sigma^2 / \epsilon$.

IV. RESULTS

A. Polymer organization and conformational statistics

We consider first the effects of confinement and crowding on the organization of the polymers in the cavity. Figure 1 shows 2-D probability distributions that characterize the position of the polymers inside the box-like cavity in the transverse plane. Results are shown for wide range of box widths. The lowest value of L was chosen to maintain the condition $L > h$, while the highest value of L (as explained below) corresponds to a system for which confinement and inter-polymer crowding effects are negligible. Row (a) shows the probability of the centre of mass of a polymer at any position in the $x - y$ plane for the case where just a single polymer is confined to the cavity. Row (b) shows the same probability distribution for the case where two identical polymers are confined to the box. We label these distributions $\mathcal{P}_1(x, y)$, where the subscript denotes the single-polymer aspect of the distribution (and *not* the number of confined polymers). Row (c) shows probability distributions for the difference in the centre-of-mass coordinates, δx and δy , of the

polymers in the two-polymer system. We label these distributions $\mathcal{P}_2(\delta x, \delta y)$, where the subscript denotes the fact that this is a 2-polymer property. (Note that this quantity is a physically meaningful descriptor only for the 2-polymer system.) Together, the two complementary distributions provide a clear picture of the effect of varying box width L on the polymer position. As an aid to interpret these 2D probability maps, Figs. 1(d), (e) and (f) show probability cross sections of $\mathcal{P}_1(x, y)$ and $\mathcal{P}_2(\delta x, \delta y)$ for some of the two-polymer systems.

A useful relative measure of the box width is the ratio $L/R_{g,xy}^*$, where $R_{g,xy}^*$ is the transverse root-mean-square radius of gyration for a polymer in a slit, i.e., $L=\infty$. A box with $L/R_{g,xy}^* \gg 1$ is large in the sense that the polymers are unlikely to interact with either the walls or with each other. As the box width approaches the regime where $L/R_{g,xy}^*$ is of the order of unity, the combined effects of the polymer-polymer and polymer-wall interactions are expected to strongly affect the organization of the polymers inside the box as well as their conformational behaviour. Note that the system in Fig. 1 is characterized by $N=60$ and $h=4$, for which $R_{g,xy}^* = 5.710 \pm 0.001$.

Let us consider first the behaviour of the 1-polymer system. At the largest box size of $L = 78$, the probability distribution $\mathcal{P}_1(x, y)$ is fairly flat over the $x - y$ plane, with the exception of an entropy-induced depletion layer along the lateral walls. As L is reduced, relative width of the depletion zone grows, and the polymer centre-of-mass distribution increasingly narrows to the box centre. Concomitantly, the distribution transforms from a square shape (corresponding to the shape of the box) to a circular shape.

A comparison of the $\mathcal{P}_1(x, y)$ distributions for the 1-polymer system with those for the 2-polymer systems shows the increasingly pronounced effect of crowding as L decreases. For the largest box size of $L = 78$ ($L/R_{g,xy}^* = 13.7$), $\mathcal{P}_1(x, y)$ is essentially identical to that for the 1-polymer system: flat over the $x - y$ plane, with an entropy-induced depletion layer along the lateral walls. This is precisely the behaviour expected in the dilute limit where interpolymer interactions are infrequent. The corresponding distribution $\mathcal{P}_2(\delta x, \delta y)$ exhibits a high-probability ring with a probability hole in the middle, as well as very low probability for large inter-polymer displacements. The depletion hole corresponds simply to the tendency of the polymers to avoid transverse overlap, as such configurations would reduce the conformational entropy. Likewise, very large separations require the polymers to press against the walls of the box, which also has an entropy-reducing effect. Within the high-probability ring, there are slight enhancements at four symmetrically distributed locations, two at $\delta x = 0$ and two at $\delta y = 0$.

As L becomes smaller, $\mathcal{P}_1(x, y)$ changes significantly. At $L=38$ ($L/R_{g,xy}^*=6.7$), small peaks appear near the corners of the distribution. Thus, the polymers increasingly tend to be situated near the corners of the box. No

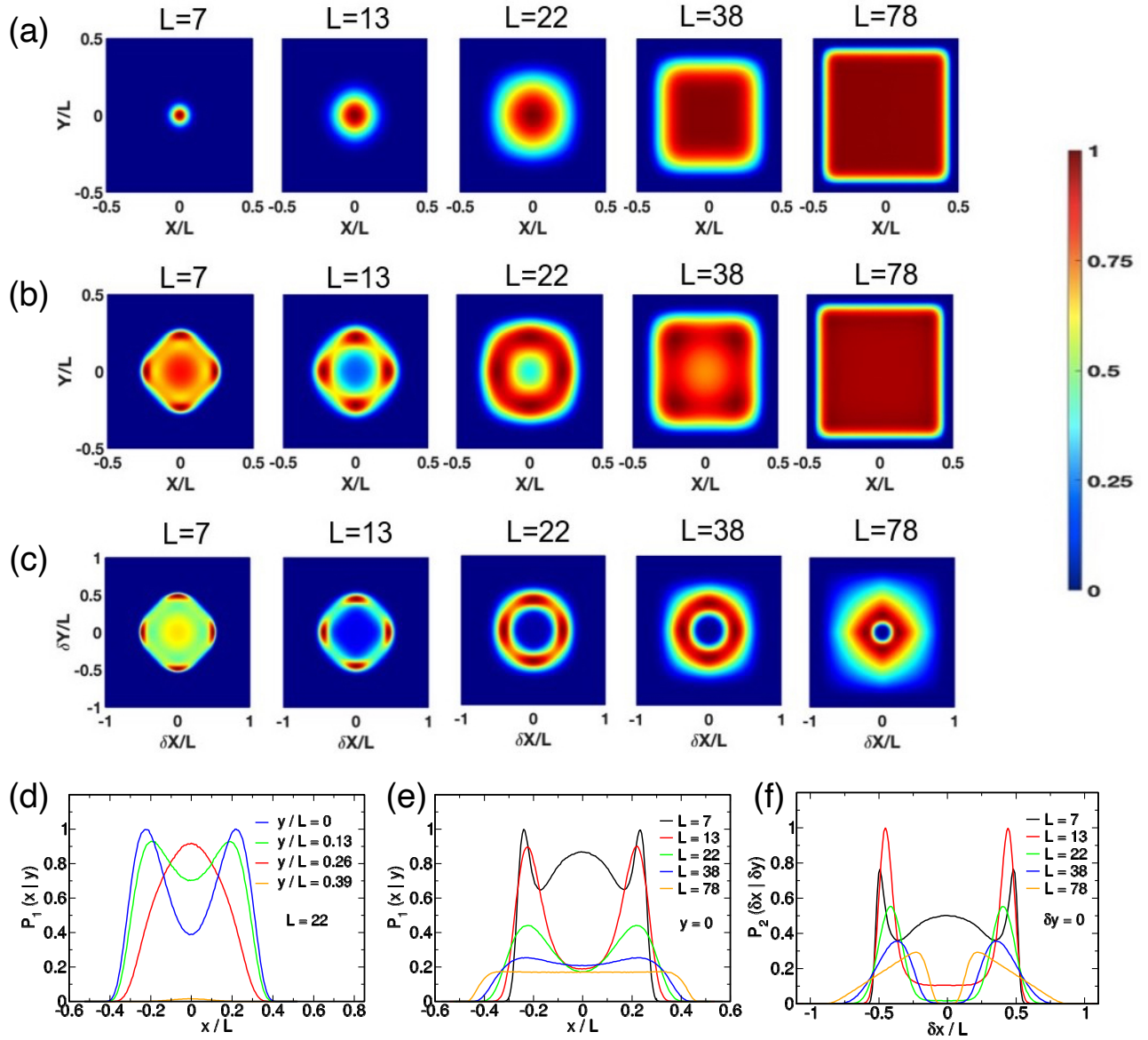


FIG. 1. Probability distributions for a system of one and two polymers of length $N=60$ confined to a box of height $h=4$. Results for various box widths are shown. Row (a) shows results for the distribution $\mathcal{P}_1(x, y)$ for a *single-polymer system*. Row (b) shows distribution $\mathcal{P}_1(x, y)$ for a *two-polymer system*. Row (c) shows $\mathcal{P}_2(\delta x, \delta y)$, the probability distributions for the *difference* in the centre-of-mass coordinates, δx and δy of the polymers in the two-polymer system. In (a), (b) and (c) the axes are scaled by the box width, L , and the colour intensity maximum corresponds to the maximum value of the probability for each graph. (d) Probability distribution cross-sections $\mathcal{P}_1(x|y)$ for the two-polymer system with $L=22$ for various values of y . (e) As in (d), except for $y=0$ (which bisects the box) for various L . (f) Probability distribution cross-sections $\mathcal{P}_2(\delta x|\delta y)$ for $\delta y=0$ and for various L .

such feature is present for the 1-polymer system, indicating that it is a consequence of interpolymer crowding. At a smaller box size $L=22$ ($L/R_{g,xy}^*=3.9$), the distribution has a ring-like structure, with a significant depletion hole in the centre of the box. Slight enhancements are evident at four symmetrically related positions. The narrowness of the ring structure for the corresponding $\mathcal{P}_2(\delta x, \delta y)$ in-

dicates that when one polymer centre lies at (x, y) the other will tend to lie at an inverted position of $(-x, -y)$. Thus, each polymer centre is expected to diffuse around the centre of the box with the other polymer moving in a correlated manner in this inverted position. Note the pronounced qualitative difference in $\mathcal{P}_1(x, y)$ between the one- and two-polymer systems.

As the box size decreases to $L=13$ ($L/R_{g,xy}^*=2.3$) the ring structure for the two distributions gives way to strong probability enhancements at four symmetrically related positions. For \mathcal{P}_1 , two are located along $x=0$ and the other two are at $y=0$. A similar structure is evident for \mathcal{P}_2 . This behaviour indicates that the polymers tend to occupy quasi-discrete locations in opposite halves of the box divided by boundaries at $x=0$ or $y=0$. Such behaviour is a consequence of the significant interaction between the polymers (i.e., crowding) and between each polymer and the confining walls (i.e., confinement) for this small box size. As will be shown below, these interactions also strongly deform the polymer conformation leading to significant changes in its average size and shape. At the smallest examined box size of $L = 7$ ($L/R_{g,xy}^*=1.23$), a new trend emerges: an enhancement of the probability at positions near the centre of the box and for very small inter-polymer displacements (i.e. near $\delta x = \delta y = 0$). Note that these broad probability peaks for $\mathcal{P}_1(x, y)$ and $\mathcal{P}_2(\delta x, \delta y)$ each coexist with the remaining four peaks associated with the quasi-discrete states described above. Again, we note the qualitatively different behaviour in $\mathcal{P}_1(x, y)$ for the 1- and 2-polymer systems for these small box sizes.

Although the distributions in Fig. 1 were calculated for $N=60$ and $h=4$, the qualitative trends are unaffected by other choices of N and h (as long as h is sufficiently small to compress the polymer along the z direction). Distributions for a polymer length of $N=300$ and box heights of $h=4, 6$, and 8 presented in Figs. 1 and 2 of the ESI indeed show the same trends as those in Fig. 1 above.†

The tendency of the polymer positions to become inversely correlated with respect to the box centre for highly confined systems is also illustrated in Fig. 2. The mean-square centre-of-mass position of each polymer, $\langle x_1^2 \rangle$ ($= \langle x_2^2 \rangle$), and the position cross-correlation, $-\langle x_1 x_2 \rangle$, both decrease monotonically with decreasing L . However, the ratio, $-\langle x_1 x_2 \rangle / \langle x_1^2 \rangle$, shown in the inset increases as the polymers become more confined. This ratio is a measure of the degree of inverse correlation of the polymer positions. Note that the ratio is independent of N when plotted against the scaled box length, $L/R_{g,xy}^*$. We expect qualitatively similar behaviour for more a realistic polymer model (e.g., one providing a better description of λ DNA), except with a much lower degree of correlation. The convergence of the ratio to unity here likely arises from packing effects due to the high volume fraction at low L .

Now let us examine conformational behaviour of each individual polymer. Figure 3 illustrates the effect of lateral confinement on the mean size and shape of the polymer. Figure 3(a) shows the variation of the transverse radius of gyration, $R_{g,xy}$, with respect to the box width. Results are shown for both 1- and 2-polymer systems for comparison. For sufficiently large L , where polymer-wall and polymer-polymer interactions are infrequent the transverse size of each polymer is close to

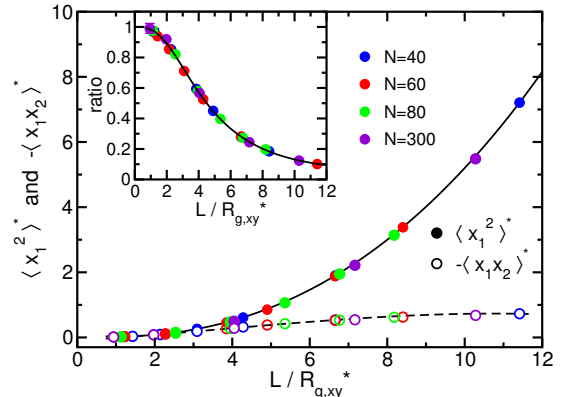


FIG. 2. Variation of $\langle x_1^2 \rangle^* \equiv \langle x_1^2 \rangle / (R_{g,xy}^*)^2$ (closed symbols) and $-\langle x_1 x_2 \rangle^* \equiv -\langle x_1 x_2 \rangle / (R_{g,xy}^*)^2$ (open symbols) with scaled box width, $L/R_{g,xy}^*$. Results are shown for $N=40, 60, 80$, and 300 . The solid and dashed curves are guides for the eye. The inset shows the ratio of the two quantities for each chain length.

the value for a slit. For $L/R_{g,xy}^* \lesssim 5$, the size decreases rapidly with decreasing L . This decrease is comparable for both 1- and 2-polymer systems, indicating that it is driven primarily by the interactions with the lateral confining walls and less so by inter-polymer crowding. The relative difference between the two sets of results, $\Delta R \equiv (R_{g,xy}(1 \text{ pol}) - R_{g,xy}(2 \text{ pol})) / R_{g,xy}$, is shown in the inset of Fig. 3(a). The difference peaks at $L \approx 4R_{g,xy}^*$, below which it decreases rapidly. Thus, at very small L , the inter-polymer crowding no longer drives compression of the polymer in the $x-y$ plane. This likely arises from the increased tendency of the polymers to overlap with each other at the centre of the box in this regime.

Fig. 3(b) shows the variation of the asphericity A_2 , defined in Eq. (10) with respect to box width. As in Fig. 3(a), the results are comparable to those for a slit when L is sufficiently large. As L decreases, increased polymer-wall and polymer-polymer interactions result in a reduction in A_2 . This implies that each polymer becomes less elongated and more disc-like as crowding increases. The difference between the 1- and 2-polymer results is shown in the inset. While qualitatively similar to the data in the Fig. 4(a) inset for the polymer size, the difference for ΔA_2 peaks at a much smaller box size of $L \approx 1.6R_{g,xy}^*$. The difference is appreciable. For example, at $L=7$ we note $\Delta A_2 = 0.13$, which is 21% of the asphericity for slit confinement. In addition, maximum ΔA_2 occurs at greatest confinement, precisely where the size difference is negligible and where Fig. 1 indicates that the polymers in the 2-polymer system have a tendency to overlap in the middle of opposite halves of the box. The concomitant inter-polymer repulsion evidently leads to a larger asphericity than for the case of a single polymer that interacts solely with the walls.

Given the effects of inter-polymer repulsion on poly-

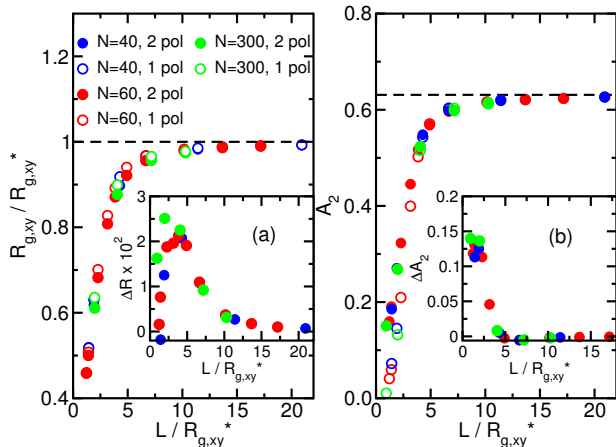


FIG. 3. (a) Scaled transverse radius of gyration, $R_{g,xy}/R_{g,xy}^*$, vs. scaled box width, $L/R_{g,xy}^*$. Results are shown for box height $h=4$ and for both 1-polymer and 2-polymer systems for $N=40, 60$ and 300 . The horizontal dashed line shows the value for $L=\infty$. The inset shows the relative difference ΔR (defined in the text) between the data for the 1- and 2-polymer systems. (b) Asphericity, A_2 , vs. scaled box width for the same systems as in panel (a). The horizontal dashed line is the value measured for a slit for $N=60$. The inset shows the difference ΔA_2 between the 1- and 2-polymer results.

mer size and shape for small and medium box widths, it is instructive to quantify the degree of polymer overlap. As described in Section III C, we define the overlap parameter $\chi_{ov} \equiv N_{ov}/N$, where N_{ov} is the mean number of monomers inside overlapping equivalent ellipses for the polymers. As a reference, we also show results for an *artificial* system of two *non-interacting* polymers, i.e., a model system in which overlap between pairs of monomers on different polymers are ignored (though non-bonded *intra*-polymer interactions are present). We refer to this as a “non-interacting” (NI) system, and the real system as an “interacting” (I) system.

Figure 4(a) shows the variation of χ_{ov} with box size for three different polymer lengths. The degree of overlap is very small for large L and increases significantly with increasing confinement. This is true for both interacting and non-interacting polymers. The values for the non-interacting system are larger than those for the interacting system. This arises simply from the entropic repulsion between polymers caused by the inter-polymer interactions. In the absence of such interactions the polymers have a greater tendency to overlap in the $x-y$ plane. For interacting polymers, the figure shows a transition in the rate of change of overlap with box width at $L/R_{g,xy}^* \approx 5$. For $L/R_{g,xy}^* \lesssim 5$ the decrease in χ_{ov} with box width is exponential characterized by a decay constant of ≈ 1.0 , while for $L/R_{g,xy}^* \gtrsim 5$ the exponential decay constant is ≈ 6.8 . Thus, the degree of overlap increases rapidly with increasing confinement in the

regime for $L/R_{g,xy}^* \lesssim 5$. This inference is corroborated by the results in Fig. 4(b), which shows the ratio of the 1- and 2-polymer values for χ_{ov} . For large box widths of $L/R_{g,xy}^* \gtrsim 5$, each ratio is small and constant. For smaller box widths of $L/R_{g,xy}^* \lesssim 5$ the ratio rapidly increases for smaller box widths. Together, the results of Fig. 4(a) and (b) indicate that the entropic repulsion preventing overlap of interacting polymers is being overridden by the even stronger repulsion from the walls, contact with which becomes increasingly unavoidable at smaller L . This region of enhanced overlap coincides with that of the dramatic reduction in size and asphericity of the polymers. Finally, in Fig. 3 of the ESI, results obtained using an alternative as a measure of overlap show the same qualitative trend as in Fig. 4(b).

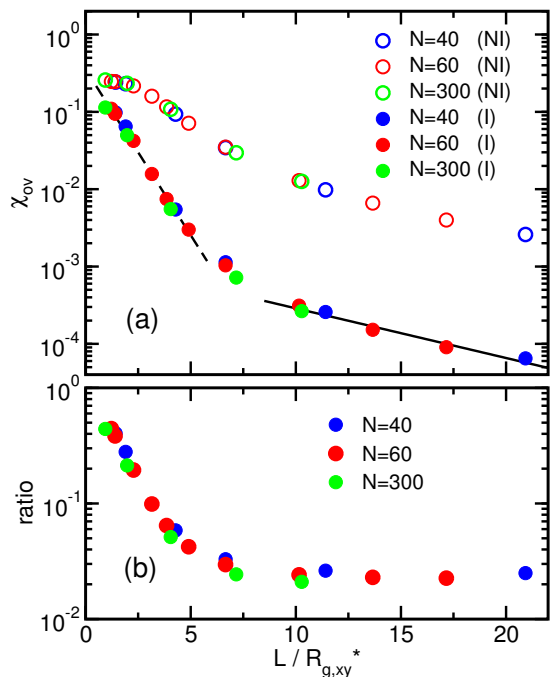


FIG. 4. (a) Variation of the overlap parameter, χ_{ov} , with scaled box width, $L/R_{g,xy}^*$. Results are shown for $N=40, 60$, and 300 for both interacting (I) and noninteracting (NI) polymer systems. The definitions of these systems is described in the text. The dashed and solid lines are fits to the interacting-system data in the regimes $L/R_{g,xy}^* < 5$ and $L/R_{g,xy}^* > 10$, respectively. (b) Ratio of the overlap parameter for the NI and I cases as a function of box width.

To summarize, the equilibrium statistics of the confined-polymer system exhibits behaviour that depends strongly on the lateral width, L , of the confining box. At $L/R_{g,xy}^* \gtrsim 5$ the polymers rarely interact with each other or with the wall, and each chain behaves in most ways comparably to a single slit-confined polymer. For smaller boxes with $L/R_{g,xy}^* \lesssim 5$, the effects of confinement and inter-polymer crowding become appreciable. As L decreases in this regime, the centres

of mass of the two become increasingly localized at positions in opposite halves of the box, except for very small boxes where there is a simultaneous tendency for them to overlap the the box centre. In addition, there is an increase in the overlap in the lateral distributions of monomers, which is driven by the increase in confinement and, counter-intuitively, enhanced by inter-polymer repulsion. We also find that increasing lateral confinement decreases the average size of the chains, an effect that is enhanced by inter-polymer crowding. The shape anisotropy (“asphericity”) also decreases with decreasing L in this regime, though this effect is slightly offset by that caused by inter-chain crowding.

B. Polymer dynamics

We now examine the equilibrium dynamics of the confined-polymer system. As in Section IV A we choose a single box height of $h=4$ and consider the effects of varying the box width. The trends in the dynamics can then be explained in the context of those for the equilibrium statistics described in the previous section. Both the diffusion of the centre of mass and the internal dynamics are characterized. As in Section IV A it is useful to consider a 1-polymer system for comparison with the 2-polymer case in order to elucidate the effects of inter-polymer repulsion on the system behaviour.

We consider first the mean-square displacement (MSD) of the polymer centre of mass, defined in Eq. (5). Figure 5(a) shows the time dependence of the MSD for a 2-polymer system with $N=60$, $L=13$. Initially, the curve rises rapidly with time, after which it levels off to a constant value of approximately 7.8. The leveling off of the MSD is a straightforward consequence of the confinement of the polymer in the lateral directions. The basic features of the MSD shown in the figure are generic to the results for all L . Generally, the limiting value of the MSD at long time and the characteristic time, τ (defined below), required to reach this plateau both increase with increasing box size. Increasing the polymer length reduces the long-time value of the MSD and increases τ .

A quantitative analysis of the MSD is aided by employing a theoretical model used in Ref. 19 to analyze comparable experimental data. In this description, the centre-of-mass motion of a single DNA molecule confined to a box-like cavity is modeled as free Brownian diffusion of a particle subject to an infinite square-well potential.⁴⁹ Interactions between polymer chains are effectively ignored, implying that the model should only be quantitatively accurate for sufficiently wide boxes. Since the cavity is symmetric in the x and y dimensions, the MSD is the same along these axes and can be averaged. Solving the diffusion equation for a single particle in a square box of side length L_e yields⁴⁹

$$\text{MSD}(t) = C_0 - C_1 \sum_{n=1,3,5,\dots}^{\infty} \frac{1}{n^4} \exp \left[-D \left(\frac{n\pi}{L_e} \right)^2 t \right] \quad (12)$$

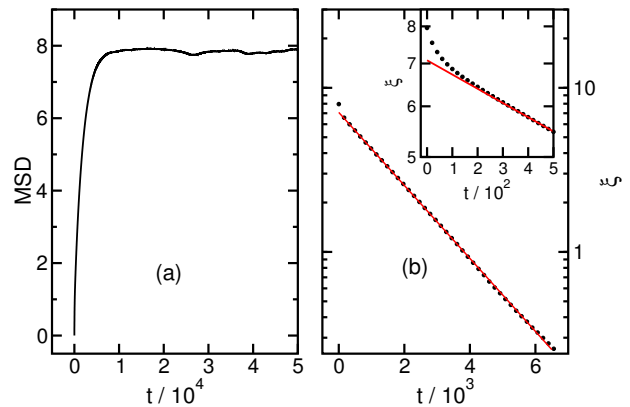


FIG. 5. (a) MSD versus time for a polymer of length $N=60$ in a box of width $L=13$ and height $h=4$. (b) ξ versus time for the system in (a), where $\xi \equiv C_0 - \text{MSD}(t)$, and where C_0 is the mean value of the MSD for $t > 20000$. The red curve is a fit to an exponential using data in the range of $t = 1000 - 6000$. The inset is a closeup of the data at small t illustrating the deviation in the exponential fit in this regime.

where D is the diffusion coefficient of the particle, and where $C_0 \equiv L_e^2/6$ and $C_1 \equiv 16L_e^2/\pi^4$. Defining the quantity $\xi(t)$ as

$$\xi(t) \equiv C_0 - \text{MSD}(t), \quad (13)$$

and noting that all of the terms with $n \geq 3$ and are negligible in comparison to the $n = 1$ term for sufficiently long t , it follows that

$$\xi(t) \approx C_1 \exp(-t/\tau) \quad (14)$$

in this long-time limit, where $\tau \equiv DL_e^2/\pi^2$.

To apply these results to the mean-square displacement of the centre of mass of a polymer diffusing in two dimensional square box, a reasonable choice of the effective box length is $L_e = L - 2R_{g,xy}^*$, where L is the true side length of the confining box and $R_{g,xy}^*$ is the radius of gyration of the polymer measured in the $x - y$ plane for a slit geometry. Thus, the polymer is modeled as a hard 2-D disk of radius $R_{g,xy}^*$, and shape deformations associated with pressing the polymer against a side wall are neglected.¹⁹ In addition, noting that Rouse dynamics are obeyed for the simulation model, it follows that $D = k_B T/\gamma$. Since the friction coefficient satisfies $\gamma = N\gamma_0$, where γ_0 is the friction per monomer, and noting that $k_B T/\gamma_0 = 1$, it follows that $D = 1/N$. Consequently, the time constant in Eq. (14) satisfies:

$$\tau/N = L_e^2/\pi^2. \quad (15)$$

Figure 5(b) shows the time dependence of the quantity ξ , calculated using the data in Fig. 5(a). Consistent with the theoretical model, we find that ξ decreases exponentially with time. Only a small deviation from

this behaviour is observed at low values of t , as illustrated in the inset of the figure. This arises from the non-negligible contribution to the MSD from the higher- n terms in Eq. (12).

Figure 6(a) shows the variation of the scaled time constant, τ/N , with respect to the scaled box length, $L/R_{g,xy}^*$, while Fig. 6(b) shows τ/N vs. the effective box length, L_e . Here, τ is extracted from the fit of ξ to Eq. (14), and the effective box with is obtained from $L_e = \sqrt{6C_0}$, where the quantity C_0 , defined in Eq. (12), is estimated from the MSD in the plateau region. Results are shown for both 1- and 2-polymer systems for polymer lengths of $N=40, 60$ and 80 . In Fig. 6(b) the theoretical prediction of Eq. (15) is shown as a dashed curve. As expected, the data for both 1- and 2-polymer systems both converge to the theoretical curve in the limit of large box length. In this regime, interactions between the two polymers are infrequent and therefore do not change the dynamical behaviour of either polymer. As L_e decreases, such interactions become more frequent, leading to a reduction in the rate of diffusion of the polymers. This is characterized by an increase in the time constant relative to both the predictions of the theoretical model and the 1-polymer time constant. Surprisingly, the prediction of Eq. (14) remains very accurate for the 1-polymer system even to very small box sizes where $L_{\text{eff}} \approx R_{g,xy}^*$.

As an additional test of the approximations employed in the theoretical model, we consider the quantity $\zeta \equiv (L - L_e)/2R_{g,xy}^*$. As noted above, the effective box width is expected to be $L_e \approx L - 2R_{g,xy}^*$ if we neglect the deformations in the size and shape of the polymer. In this picture, ζ is a constant of order unity. The inset of Fig. 6(b) shows the measured variation of ζ with $L/R_{g,xy}^*$ for both 1- and 2-polymer systems. For the single-polymer system, ζ is indeed constant and close to unity for $L/R_{g,xy}^* \gtrsim 5$. However, for $L/R_{g,xy}^* \lesssim 5$, ζ decreases slightly with decreasing box width. In this regime, there is no extended area in the $x-y$ plane over which the polymer centre of mass can move without interacting with the walls. Thus, size and shape deformations are significant and neglecting them leads to the observed deviation from the prediction.

A similar trend is observed for the 2-polymer system. However, in this case the transition occurs at a larger box width of $L/R_{g,xy}^* \approx 10$. The additional crowding caused by the presence of the second polymer leads to increased interaction with the lateral walls as well as shape deformations at box sizes where such effects are not as prominent in the 1-polymer system. Note that the 2-polymer ζ begins to decrease significantly with decreasing L at $L/R_{g,xy}^* \approx 5$, which corresponds to $L \approx 29$ and $L_e \approx 17$. This is precisely where the measured τ/N for the 2-polymer system begins to deviate from the dilute-limit approximation.

Next, we examine the time dependence of correlations in the centre-of-mass positions of the polymers. We use the autocorrelation function, $C_{\text{auto}}(t)$, and cross-correlation function, $C_{\text{cross}}(t)$, defined in Eqs. (6) and

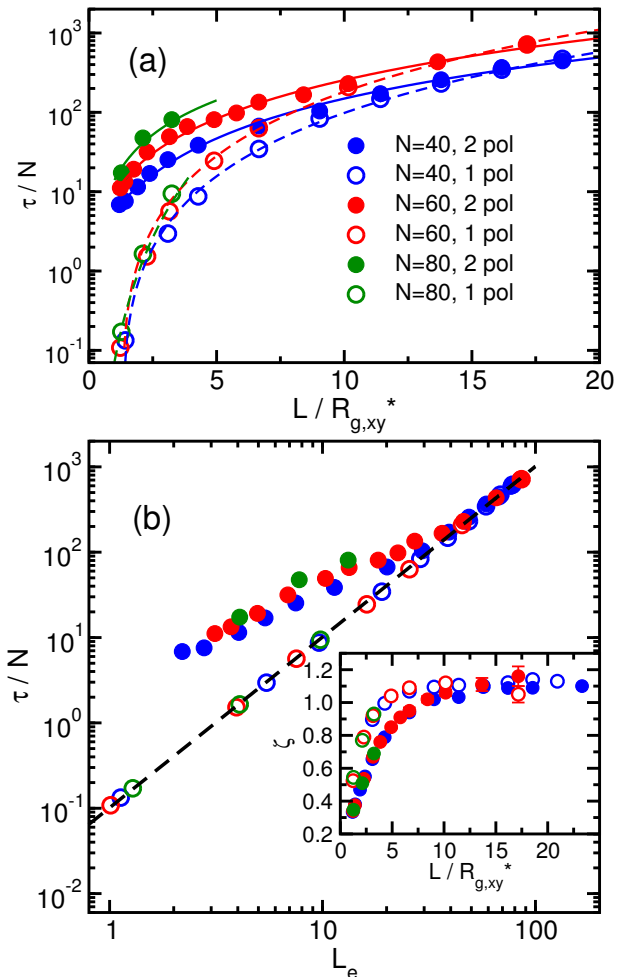


FIG. 6. (a) Variation of τ/N with respect to $L/R_{g,xy}^*$. The time constant τ is extracted from fits to $\xi(t)$ at sufficiently long times, where $\xi(t) \equiv C_0 - \text{MSD}(t)$, and where $C_0 = \lim_{t \rightarrow \infty} \text{MSD}(t)$. Results are shown for systems of a single polymer (open symbols) and for two polymers (closed symbols) and for polymer lengths of $N=40, 60$ and 80 . The solid and dashed lines are guides for the eye for 2-polymer and 1-polymer data sets, respectively. (b) τ/N vs. L_e , where the effective box width is defined $L_e = \sqrt{6C_0}$, as discussed in the text. The dashed line shows the prediction of Eq. (15), which is expected to be valid at $L_e/R_{g,xy}^* \gg 1$. The inset shows the variation of $\zeta \equiv (L - L_e)/2R_{g,xy}^*$ with $L/R_{g,xy}^*$.

(7), respectively. Figure 7 shows both functions for box widths of $L=13, 22$, and 33 . Both correlation functions tend decay exponentially at large t . Note that in each case the decay to zero at long t is a consequence of choosing $x = y = 0$ at the box centre. The individual functions diverge with decreasing t . This divergence is greater for larger box sizes.

The system behaviour at $t = 0$ has a simple explanation. Note that $C_{\text{auto}}(0) = \langle x_1^2 \rangle$ and $C_{\text{cross}}(0) = -\langle x_1 x_2 \rangle$. As previously noted for the results in Fig. 2, $\langle x_1^2 \rangle$ ap-

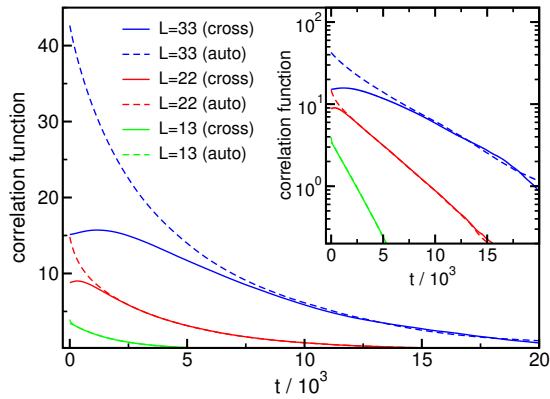


FIG. 7. Autocorrelation function, $C_{\text{auto}} \equiv \langle x_1(t)x_1(0) \rangle$, and cross-correlation function, $C_{\text{cross}} \equiv -\langle x_1(t)x_2(0) \rangle$, for the centre-of-mass positions for two $N=60$ polymers. Results are shown for $L=13, 22$, and 33 . The inset shows the same data plotted on a semi-log scale.

proaches $-\langle x_1x_2 \rangle$ for small box sizes since the polymer positions in the $x-y$ plane are highly anti-correlated in this regime (i.e. if one polymer lies at (x, y) the other is likely to be near $(-x, -y)$). For larger box sizes the degree of anticorrelation is smaller, leading the observed wider divergence between the correlation functions for larger L .

To better understand the origins of the observed time dependence of the functions, we employ a simple model to describe the box-size regime where the polymers are pushed out from the centre of the box (see, e.g., the results for $L=13$ and $L=22$ in Fig. 1). Here, the polymers are pictured as two point particles that each occupy one of four discrete sites on the corners of a square and whose interactions mimic the effects of entropic repulsion. The model can be used in MC dynamics simulations to measure the two position correlation functions. The model is fully described in the appendix, and the calculated correlation functions are shown in Fig. 9. The convergence to exponential decay at large t and the divergence at low t are both present. Thus, a simple model incorporating the basic features of the probability distributions of Fig. 1 and a simple description of entropic repulsion between the polymers is capable of accounting for the general behaviour of the correlation functions.

Let us now examine the effects of confinement on the internal motion of the polymers. A useful means to characterize such motion is the autocorrelation function of the Rouse coordinates of the polymer. As noted in Section III, these functions tend to be exponential over at least one decade of decay (except at very short times) for both 1- and 2-polymer systems.

Figure 8(a) shows the variation of the Rouse mode correlation times for the $p=1$ mode with respect to box width. Note that τ_1 describes rates of conformational motion on large length scales. For sufficiently wide boxes

τ_1 approaches the value for slit confinement for both 1- and 2-polymer systems. Thus, the rate of conformational change is independent of box width when the polymers rarely encounter the confining walls. However, as L decreases, the behaviours of the two systems diverge. For the 2-polymer system the τ_1 exhibits a peak at $L/R_{g,xy}^* \approx 4$, followed by a sharp decrease at lower L . By contrast, the 1-polymer system has no maximum in this region, and instead τ_1 exhibits solely a sharp decrease at $L/R_{g,xy}^* \lesssim 5$.

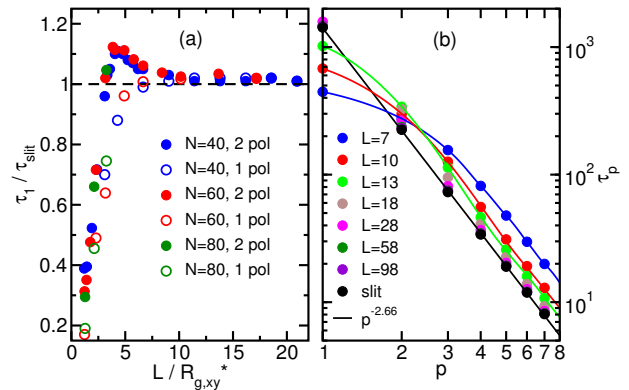


FIG. 8. (a) Variation of scaled Rouse mode correlation time $\tau_1/\tau_{\text{slit}}$ with box width, L , where τ_{slit} is the value of τ_1 for slit confinement. Results are shown for $N=60$ for 1- and 2-polymer systems. The dashed line corresponds to $\tau_1 = \tau_{\text{slit}}$. (b) Variation of τ_p with mode index p for a 2-polymer system with $N=60$. Results are shown for various box widths. The black curve shows a fit to the results for slit-confinement ($L = \infty$) to a power law. The other curves are guides for the eye for $L=6, 8$, and 13 .

The effect of confinement on Rouse mode relaxation has been previously examined analytically using a Gaussian chain subject to a harmonic confining potential.⁵⁰ In each dimension subject to this confinement, it was shown that $C_p(t)$ decays exponentially with a relaxation time

$$1/\tau_p = 1/\tau_p^{(0)} + 1/\tau_e, \quad (16)$$

where $\tau_p^{(0)} \propto (N/p)^2$ is the relaxation time for an unconfined chain, and τ_e is a constant proportional to \bar{d}^2 , where \bar{d} is the effective confinement width. Thus, in this model τ_p decreases as the confinement increases, qualitatively consistent with the present results for τ_1 for a single self-avoiding chain laterally confined between hard walls. The presence of a second polymer chain effects an increase in τ_1 over the range of L where the two polymers are forced to be in contact with each other, including lower values of L where $\tau_1 < \tau_{\text{slit}}$. This is likely an effect of polymer crowding impeding conformational motion on large length scales. The competition between the effects of confinement, which tends to decrease τ_1 , and crowding, which tends to increase τ_1 , leads to the local maximum.

Figure 8(b) shows the variation of the Rouse mode correlation times, τ_p , as a function of mode index p for the 2-polymer system with $N=60$. Results are shown for various box widths for mode indices in the range $p = 1 - 7$. In all cases τ_p decreases monotonically with p . For confinement to a slit, i.e. $L = \infty$, the results exhibit power-law behaviour with $\tau_p \propto p^{-2.66}$. This is close to the expected Rouse scaling for a 2-D polymer in good solvent conditions: $\tau_p \propto p^{-(1+2\nu)} = p^{-2.5}$, where $\nu = 0.75$ is the Flory scaling exponent for two dimensions.⁵¹ The discrepancy is likely a result of finite-size effects. The relaxation times τ_p are independent of L for $L \gtrsim 20$. For $L \lesssim 20$ ($L/R_{g,xy}^* \lesssim 3.5$), τ_p increases with decreasing box width for all p except for the case of $p = 1$ at very small L , as noted above. Thus, in the confinement regime where 2-polymer crowding effects become noticeable, the conformational dynamics appear to be slowed over all length scales. Finally, we speculate that $\tau_p < \tau_p^{(\text{slit})}$ for $p \geq 2$ for smaller box widths than those examined in our simulations. This follows from the fact that Eq. (16) suggests that as p increases the second term in Eq. (16) can remain appreciable relative to the first term if the confinement dimension \tilde{d} (analogous to L) is reduced.

To summarize, we find that the dynamics of the confined-polymer system are significantly affected by size of the confining cavity for sufficiently small L . The centre-of-mass motion and the conformational dynamics are both influenced by a combination of confinement effects that are also present for a single polymer, as well as crowding effects arising from interactions between the two polymers. These effects become pronounced precisely in the regime where the centre-of-mass probability distributions, the average size and shape of individual polymers, and the degree of polymer overlap are also strongly altered.

V. RELEVANCE TO EXPERIMENT

As noted in the introduction, this study is principally motivated by the recent work of Capaldi *et al.*,¹⁹ who used optical imaging methods to probe the organization and dynamics of DNA molecules trapped in nanofluidic cavities. Consequently, it is of value to examine the relevance of the results of the present study to those experiments.

It is important to first note how the choice of model limits direct quantitative comparison. In their experiments using fluorescently stained λ DNA, Capaldi *et al.* used a solution containing 10 mM tris at pH 8 with 2% BME, corresponding to an ionic strength of about $I = 12$ mM. Using the empirical relation between the Kuhn length, l_K , and ionic strength from Dobrynin⁵² we estimate $l_K \approx 100$ nm. Likewise, using the theory of Stigter⁵³ for the relation between the I and the effective chain width, w , we estimate $w \approx 10$ nm, and thus the monomer anisotropy ratio is $l_K/w \approx 10$. For the staining ratio of 10:1 (bp:fluorophore) employed, the Kuhn length

is not expected to change.⁵⁴ On the other hand, the contour length is expected to increase due to unwinding of the double helix. From Fig. 7 of Ref. 54 we estimate that a 10:1 YOYO-1 staining ratio leads to a contour length increase of about 15%. As unstained λ DNA has a contour length of $L_c = 16.5 \mu\text{m}$, the value for stained DNA is expected to be $L_c \approx 19 \mu\text{m}$. Thus, we estimate a ratio of $L_c/l_K \approx 190$. The simulation model employed a flexible chain of spherical beads. If the bead width (which is approximately the mean bond length) represents one Kuhn length, then the model polymers should have a length of $N=190$ to achieve the correct L_c/l_K ratio. This is larger by a factor of 2.4–5 than the polymer lengths ($N=40$ –80) used in most simulations, with the exception of some calculations for $N=300$ carried out in MC simulations. More problematic is the ratio of $l_K/w = 1$ in the simulation model. Finally, the ratio of the bulk radius gyration ($\approx 700 \text{ nm}$ ⁵⁵) to the nanofluidic cavity depth (200 nm) is $R_g/h \approx 3.5$. By contrast, the ratio for the simulation model using $N=60$ and $h=4$ is $R_g/h \approx 1.35$. Thus, confinement in the narrow dimension of the cavity deforms λ -DNA significantly more than is the case in the model system. Increasing the ratio by decreasing h in the simulation leads to small ratios of h/w that result in unacceptable artifacts. Choosing model parameter values to better match the other length scale ratios to those in the experiments leads to simulations that require infeasibly long simulation times, especially in the case of Brownian dynamics simulations. Consequently, we must use a model system for which we can expect only qualitative or, at best, semi-quantitative agreement between experiment and simulation.

The simulations examined cavities with a wide range of width values. By contrast the nanocavities employed in the experiments had a single fixed width of $2 \mu\text{m}$. The ratio of the in-plane radius of gyration ($0.91 \mu\text{m}$) for a slit confined λ -DNA molecule and box length was $L/R_{g,xy}^* \approx 2.2$. Imposing this ratio on the simulation model with $N=60$ (for which $R_{g,xy}^* \approx 5.7$) implies a box width of $L \approx 13$. Figure 1 shows that a single molecule confined to a box of this width is expected to have its centre of mass be strongly localized to the centre of the box. This is qualitatively consistent with the experimental results presented in Fig. 4(a) and 4(c) of Ref. 19. The wider, more square-like distribution for the larger box sizes in Fig. 1(a) better resemble the measured position distribution for confinement of a single plasmid shown in Fig. 5(a) of Ref. 19. Since the plasmid contour length was considerably shorter than that of the λ DNA chain and was of circular topology, its average size was also much smaller. This naturally results in a distribution better approximated by a model system using a larger $L/R_{g,xy}^*$ ratio.

In the case of two confined polymers, the results for $L=13$ in Fig. 1 suggest that crowding effects cause the polymer centres to be pushed out from the centre to opposite halves of the box at four quasi-discrete locations and leaving a probability “hole” at the box centre. The

corresponding experimental results of Fig. 4(d) of Ref. 19 do indicate a crowding-induced displacement of the λ -DNA molecules from the box centre. However, in that case an asymmetry was noted, likely a result of an underlying difference in the DNA contour and persistence lengths caused by using different stains, as required for separate observation of each molecule. Specifically, the YOYO-3 labeled DNA chain was slightly more concentrated in the cavity centre than the YOYO-1 labeled chain. In addition, the distribution of sampled centre-of-mass positions shown in Fig. 4(b) of Ref. 19 do not show any evidence of the quasi-discrete states, which likely arise from enhanced packing effects due to the small value of l_K/w ratio in the model. Instead, those results are more qualitatively consistent with our simulation results for a slightly larger box width ($L=22$), where \mathcal{P}_1 tends to be dependent on radial distance from the box centre alone, independent of the polar angle, and where the probability hole at the centre is less pronounced. Such a distribution is also consistent with a collective Brownian rotation of the two molecules around the centre of the box, a behaviour noted in Ref. 19.

In addition to measurement of the time-dependence of the MSD, Capaldi *et al.* also measured the position auto-correlation function, $C_{\text{auto}}(t)$, and observed exponential decay for both 1- and 2-polymer systems. They found a time constant of $\tau = 0.25 \pm 0.01$ s for 1-chain confinement and $\tau = 2.0 \pm 0.1$ s for 2-chain confinement. Thus, the crowding effect caused by the presence of the second chain increased τ by a factor of 8. It is easy to show that an exponential decay of the correlation function implies an exponential decay of the MSD with exactly the same time constant. Figure 6 shows that the values of the time constant extracted from fits to the MSD diverge for the two different systems as L_e decreases. This divergence begins at an effective box length of $L_e \approx 20$. As noted above, the cavity width in the experiment satisfies $L/R_{g,xy}^* \approx 2.2$. For the model system, Fig. 6(a) shows that this ratio corresponds to the regime where the presence of a second polymer increases the time constant relative to the case for single-polymer confinement. Using the data in this figure we estimate an increase in the time constant by a factor of 21 for $N=60$. While this is larger than the experimental value, the model does correctly predict an increase in τ by about an order of magnitude for the two-polymer system. Given the simplicity of the molecular model, this is a reasonably good agreement.

A final point of comparison with the experiments is the relationship between the center-of-mass auto- and cross-correlation functions. Capaldi *et al.* reported exponential decay of both $C_{\text{auto}}(t)$ and $C_{\text{cross}}(t)$ with time constants of 2.0 ± 0.1 s and 2.8 ± 0.3 s, respectively. This stands in contrast to the simulation results in which exponential decay only occurs at longer time, where the two functions converge and thus are characterized by the same time constant. We suspect that this discrepancy arises from the way in which the fit to the data was carried out in Ref. 19. The cross-correlation function in

Fig. 7(c) of Ref. 19 appears to show a flattening of the curve at low t . This trend is consistent with our simulation results, suggesting that it has a physical origin and is not merely a statistical anomaly. Discarding the low- t experimental data will likely increase the measured rate of decay and thus decrease the time constant. We speculate that such a modified fit could lead to a time constant that better matches that for the autocorrelation function.

VI. CONCLUSIONS

In this study we have used MC and Brownian dynamics simulations to probe the organization, conformational behaviour, and equilibrium dynamics of two polymers under confinement in a box-like cavity with very strong confinement in one of the dimensions. We find the behaviour is highly dependent on the degree of lateral confinement. For large box width, L , where the polymers rarely interact with each other or the lateral walls, the polymer conformational statistics and dynamics are comparable to those for a single slit-confined polymer. The combined effects of confinement and inter-polymer crowding are noticeable when $L/R_{g,xy}^* \lesssim 5$, where $R_{g,xy}^*$ is the transverse radius of gyration for the case $L \rightarrow \infty$ (i.e., confinement to a slit with a spacing equal to the height of the confining cavity). In this box size regime, there is a probability hole at the box centre, and the polymer centre-of-mass positions tend to be inversely correlated with respect to the box centre (i.e. when one polymer is at position (x, y) the other tends to be at $(-x, -y)$, where the box centre is at $(0, 0)$). At lower L , the polymers tend to occupy four quasi-discrete states in opposite sides of the box, and at very small L there is an increasing tendency for polymer overlap at the box centre. The polymer size decreases with L in this regime, principally as a consequence of confinement rather than interpolymer crowding. Increasing confinement tends to reduce the 2D asphericity, though the interpolymer crowding tends to offset this effect. Both the rate of diffusion and the internal dynamics of each polymer is significantly impacted by the presence of the other polymer. Note that the transition location of $L/R_{g,xy}^* \approx 5$ is likely specific to the model employed in this study. For other models (e.g. one using semiflexible chains) the transition will likely occur at a somewhat different location, though still with $L/R_{g,xy}^*$ somewhat greater than unity.

The simple molecular model employed in this study facilitates the study of a number of generic effects of confinement on the organization and dynamics of two cavity-confined polymers. Generally, the observed behaviour is qualitatively consistent with the results of the recent experimental study by Capaldi *et al.*, which examined two λ -DNA chains confined to a nanofluidic cavity.¹⁹ We view the present study as a first step toward a more realistic modeling of such experimental systems. In principle, scaling up the polymer length and incorporating bending rigidity into the model can be used to obtain cor-

rect lengthscale ratios for the contour length, persistence length, effective width of λ DNA, and the cavity dimensions. In practice, however, the required simulation times for such a model are infeasible at present, at least for the dynamics. A promising alternative approach could be to model each polymer as a chain of blobs with diameter equal to the box height, each interacting with other blobs via a soft repulsive potential arising from entropic repulsion. This potential could be determined using a technique to measure free energy functions employed in other recent studies.^{35,37,40} Such effective potentials were recently employed to model the entropic repulsion of side-loops in a model for a bacterial chromosome.^{56,57} We anticipate that such future studies in addition to the present one will be helpful in elucidating recent experimental results as well motivating new nanofluidics experiments for cavity-confined DNA systems.

Appendix A: Position correlation functions for a discrete-site model

To better understand the behaviour of the position correlation functions shown in Fig. 7, we carry out MC dynamics simulations using a discrete-site toy model that incorporates only the most basic features of the polymer system. The two polymers are modeled as interacting particles that can each occupy one of four discrete sites on the corners of a square in the $x - y$ plane. We are most interested in the behaviour for intermediate box widths that correspond roughly to the experimental regime. Here, the polymer centres are pushed out from the box centre in opposite directions by roughly the same distance (e.g. see probability distributions for $L=13$ and $L=22$ in Fig. 1(b)). As a very simple approximation to that picture, we choose the four site positions to be $(1, 0)$, $(0, 1)$, $(-1, 0)$, and $(0, -1)$. The particles interact with an energy $E \geq 0$ that is a measure of the entropic repulsion of the polymers. The interaction energy is $E = 0$ when the particles are at opposite corners of the square, $E = E_1 (> 0)$ when the particles are on neighbouring corners, and $E = E_2 (> E_1)$ when the particles occupy the same site. Thus, the energy decreases in strength with increasing distance, in accord with the expected behaviour for entropic repulsion between polymers.

We perform a MC dynamics simulation on this system as follows. Each trial move consists of displacing a randomly chosen particle to either one of the two neighbouring sites. Each of these two neighbouring sites has equal probability of being selected. The trial move is accepted or rejected according to the Metropolis criterion. The simulation is carried out for 10^6 MC cycles, where each MC cycle consists of two trial moves. The position auto- and cross-correlation functions defined in Section IV B are calculated using the particle coordinates, which are sampled each MC cycle. Time is measured in MC cycles.

Figure 9 shows the position correlation functions using interaction energies of $E_1/k_B T = 1$ and $E_2/k_B T = 2$. As

was the case for the correlation functions for a system of two confined polymers shown in Fig. 7, $C_{\text{auto}}(t)$ and $C_{\text{cross}}(t)$ converge and decay exponentially to zero at long times. Also consistent is the behaviour at short times, where the functions diverge with $C_{\text{cross}}(t) < C_{\text{auto}}(t)$.

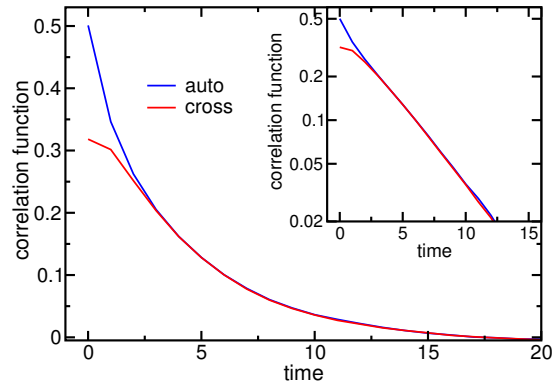


FIG. 9. Position auto-correlation and cross-correlation functions for the discrete-site model described in the text of the appendix. The inset shows the same data plotted on a semi-log scale.

Qualitatively similar behaviour is observed for other choices of E_1 and $E_2 (> E_1)$. Decreasing the interactions energies corresponds to decreasing the entropic repulsion between polymers as a result of increasing the box size, L . Generally, we find that the divergence between the $C_{\text{auto}}(t)$ and $C_{\text{cross}}(t)$ at low t is larger when the repulsion is weaker, consistent with the trend for increasing L in Fig. 7. The results presented in this appendix demonstrate that the general behaviour of the correlation functions can be accounted for using a model incorporating the qualitative features of the probability distributions of Fig. 1 as well as a simple description of entropic repulsion between the polymers.

ACKNOWLEDGMENTS

This work was supported by the Natural Sciences and Engineering Research Council of Canada (NSERC). We are grateful to Compute Canada for use of their computational resources. DR would like to thank Zhezhou Liu for helpful discussions. We would also like to thank Alex Klotz for helpful discussions and for a critical reading of the manuscript.

- ¹L. Dai, C. B. Renner, and P. S. Doyle, *Adv. Colloid Interface Sci.* **232**, 80 (2016).
- ²W. Reisner, J. N. Pedersen, and R. H. Austin, *Rep. Prog. Phys.* **75**, 106601 (2012).
- ³K. D. Dorfman, S. B. King, D. W. Olson, J. D. Thomas, and D. R. Tree, *Chem. Rev.* **113**, 2584 (2012).
- ⁴W. Reisner, N. B. Larsen, A. Silahatoglu, A. Kristensen, N. Tommerup, J. O. Tegenfeldt, and H. Flyvbjerg, *Proc. Natl. Acad. Sci. USA* **107**, 13294 (2010).

- ⁵R. Marie, J. N. Pedersen, D. L. Bauer, K. H. Rasmussen, M. Yusuf, E. Volpi, H. Flyvbjerg, A. Kristensen, and K. U. Mir, *Proc. Natl. Acad. Sci. USA* **110**, 4893 (2013).
- ⁶E. T. Lam, A. Hastie, C. Lin, D. Ehrlich, S. K. Das, M. D. Austin, P. Deshpande, H. Cao, N. Nagarajan, M. Xiao, and P.-Y. Kwok, *Nature Biotech.* **30**, 771 (2012).
- ⁷A. R. Hastie, L. Dong, A. Smith, J. Finklestein, E. T. Lam, N. Huo, H. Cao, P.-Y. Kwok, K. R. Deal, and J. Dvorak, *PLoS one* **8**, e55864 (2013).
- ⁸K. D. Dorfman, *AICHE J.* **59**, 346 (2013).
- ⁹V. Müller and F. Westerlund, *Lab Chip* **17**, 579 (2017).
- ¹⁰A. R. Klotz, M. Mamaev, L. Duong, H. W. de Haan, and W. W. Reisner, *Macromolecules* **48**, 4742 (2015).
- ¹¹A. R. Klotz, L. Duong, M. Mamaev, H. W. de Haan, J. Z. Chen, and W. W. Reisner, *Macromolecules* **48**, 5028 (2015).
- ¹²M. B. Mikkelsen, W. Reisner, H. Flyvbjerg, and A. Kristensen, *Nano Lett.* **11**, 1598 (2011).
- ¹³D. Kim, C. Bowman, J. T. Del Bonis-O'Donnell, A. Matzavinos, and D. Stein, *Phys. Rev. Lett.* **118**, 048002 (2017).
- ¹⁴C. L. Smith, A. H. Thilsted, J. N. Pedersen, T. H. Youngman, J. C. Dyrnum, N. A. Michaelsen, R. Marie, and A. Kristensen, *ACS Nano* **11**, 4553 (2017).
- ¹⁵A. R. Klotz, H. W. de Haan, and W. W. Reisner, *Phys. Rev. E* **94**, 042603 (2016).
- ¹⁶J. Del Bonis-O'Donnell, W. Reisner, and D. Stein, *New J. Phys.* **11**, 075032 (2009).
- ¹⁷A. R. Klotz, H. B. Brandao, and W. W. Reisner, *Macromolecules* **45**, 2122 (2012).
- ¹⁸F. Ruggeri and M. Krishnan, *Phys. Rev. E* **96**, 062406 (2017).
- ¹⁹X. Capaldi, Z. Liu, Y. Zhang, L. Zeng, R. Reyes-Lamothe, and W. Reisner, *Soft Matter* **14**, 8455 (2018).
- ²⁰S. Jun and B. Mulder, *Proc. Natl. Acad. Sci. USA* **103**, 12388 (2006).
- ²¹I. Teraoka and Y. Wang, *Polymer* **45**, 3835 (2004).
- ²²S. Jun, A. Arnold, and B.-Y. Ha, *Phys. Rev. Lett.* **98**, 128303 (2007).
- ²³A. Arnold and S. Jun, *Phys. Rev. E* **76**, 031901 (2007).
- ²⁴J. L. Jacobsen, *Phys. Rev. E* **82**, 051802 (2010).
- ²⁵Y. Jung and B.-Y. Ha, *Phys. Rev. E* **82**, 051926 (2010).
- ²⁶Y. Jung, C. Jeon, J. Kim, H. Jeong, S. Jun, and B.-Y. Ha, *Soft Matter* **8**, 2095 (2012).
- ²⁷Y. Jung, J. Kim, S. Jun, and B.-Y. Ha, *Macromolecules* **45**, 3256 (2012).
- ²⁸Y. Liu and B. Chakraborty, *Phys. Biol.* **9**, 066005 (2012).
- ²⁹J. Dorier and A. Stasiak, *Nucleic Acids Res.* **41**, 6808 (2013).
- ³⁰D. Račko and P. Cifra, *J. Chem. Phys.* **138**, 184904 (2013).
- ³¹J. Shin, A. G. Cherstvy, and R. Metzler, *New J. Phys.* **16**, 053047 (2014).
- ³²E. Minina and A. Arnold, *Soft Matter* **10**, 5836 (2014).
- ³³E. Minina and A. Arnold, *Macromolecules* **48**, 4998 (2015).
- ³⁴Y. Chen, W. Yu, J. Wang, and K. Luo, *J. Chem. Phys.* **143**, 134904 (2015).
- ³⁵J. M. Polson and L. G. Montgomery, *J. Chem. Phys.* **141**, 164902 (2014).
- ³⁶Y. Du, H. Jiang, and Z. Hou, *J. Chem. Phys.* **149**, 244906 (2018).
- ³⁷J. M. Polson and D. R.-M. Kerry, *Soft Matter* **14**, 6360 (2018).
- ³⁸W. Nowicki, *J. Chem. Phys.* **150**, 014902 (2019).
- ³⁹W. Nowicki, *J. Mol. Model.* **25**, 269 (2019).
- ⁴⁰J. M. Polson and Q. Zhu, *Phys. Rev. E* **103**, 012501 (2021).
- ⁴¹S. Jun and A. Wright, *Nat. Rev. Microbiol.* **8**, 600 (2010).
- ⁴²B. Di Ventura, B. Knecht, H. Andreas, W. J. Godinez, M. Fritsche, K. Rohr, W. Nickel, D. W. Heermann, and V. Sourjik, *Mol. Syst. Biol.* **9**, 686 (2013).
- ⁴³B. Youngren, H. J. Nielsen, S. Jun, and S. Austin, *Genes Dev.* **28**, 71 (2014).
- ⁴⁴J. Mannik, D. E. Castillo, D. Yang, G. Siopsis, and J. Männik, *Nucleic Acids Res.* **44**, 1216 (2016).
- ⁴⁵J. A. Cass, N. J. Kuwada, B. Traxler, and P. A. Wiggins, *Biophys. J.* **110**, 2597 (2016).
- ⁴⁶L. J. Wu, S. Lee, S. Park, L. Eland, A. Wipat, S. Holden, and J. Errington, *Nat. Commun.* **11**, 1 (2020).
- ⁴⁷N. El Najjar, D. Geisel, F. Schmidt, S. Dersch, B. Mayer, R. Hartmann, B. Eckhardt, P. Lenz, and P. L. Graumann, *mSphere* **5**, e00255 (2020).
- ⁴⁸A. Japaridze, C. Gogou, J. W. Kerssemakers, H. M. Nguyen, and C. Dekker, *Nat. Commun.* **11**, 1 (2020).
- ⁴⁹A. Kusumi, Y. Sako, and M. Yamamoto, *Biophys. J.* **65**, 2021 (1993).
- ⁵⁰A. Denissov, M. Kroutieva, N. Fatkullin, and R. Kimmich, *J. Chem. Phys.* **116**, 5217 (2002).
- ⁵¹P. de Gennes, *Scaling Concepts in Polymer Physics* (Cornell University Press, Ithaca NY, 1979).
- ⁵²A. V. Dobrynin, *Macromolecules* **39**, 9519 (2006).
- ⁵³D. Stigter, *Biopolymers* **16**, 1435 (1977).
- ⁵⁴B. Kundukad, J. Yan, and P. S. Doyle, *Soft matter* **10**, 9721 (2014).
- ⁵⁵P.-K. Lin, J.-F. Chang, C.-H. Wei, P. Tsao, W. Fann, Y.-L. Chen, *et al.*, *Phys. Rev. E* **84**, 031917 (2011).
- ⁵⁶F. Wu, P. Swain, L. Kuijpers, X. Zheng, K. Felter, M. Guurink, J. Solari, S. Jun, T. S. Shimizu, D. Chaudhuri, *et al.*, *Curr. Biol.* **29**, 2131 (2019).
- ⁵⁷P. Swain, B. M. Mulder, and D. Chaudhuri, *Soft Matter* **15**, 2677 (2019).